

Conformational and Stereodynamic Behavior of Five- to Seven-Membered 1-Aryl-2-iminoazacycloalkanes

Jimena E. Díaz,^{†,‡} Andrea Mazzanti,[†] Liliana R. Orelli,^{*,‡} and Michele Mancinelli^{*,†}

[†]Department of Industrial Chemistry “Toso Montanari”, University of Bologna, Viale Risorgimento 4, 40136 Bologna, Italy

[‡]Departamento de Química Orgánica. Facultad de Farmacia y Bioquímica, Universidad de Buenos Aires. CONICET, Junín 956, 1113 Buenos Aires, Argentina

Supporting Information



ABSTRACT: The stereodynamic behavior of 1-arylpyrrolidin-2-imines, having a $C_{aryl}-N$ stereogenic axis, has been studied by means of dynamic nuclear magnetic resonance and density functional theory calculations, evaluating the steric effect of *ortho*-aryl substituents. The rotational barrier due to *E/Z* isomerism about the $-C=N-H$ bond was also determined. The dynamic stereochemistry of homologous six- and seven-membered iminoazacycloalkane rings and their oxo-analogues was also comparatively investigated, evidencing a ring size effect. It was found that the seven-membered heterocycle shows additional dynamic features because of ring inversion.

INTRODUCTION

Many drugs containing small-ring nitrogen heterocycles exhibit a wide range of biological activities,¹ and it is widely reported that the potency and selectivity are strongly sensitive to the conformational constraints, as the ring size enlarges from five to seven members. The combination of ring size and the appropriate spatial and steric properties of the substituents bonded to the ring lead to the preparation of potent and selective drugs of great interest in medicinal chemistry. In particular, 2-iminoazaheterocycles are potent inhibitors of human nitric oxide synthase (iNOS),² and a recent synthesis of 1-aryl-2-iminoazacycloalkanes from ω -halonitriles using polyphosphoric acid esters such as ethyl polyphosphate (PPE) or trimethylsilyl polyphosphate (PPSE)³ gave the possibility to study the conformational behavior about the *N*-aryl stereogenic axis in five to seven membered heterocyclic rings. These compounds can be easily converted into their oxo-analogues by exposure to air (Scheme 1). Examples of dynamic conformational analysis due to a $C_{sp^2}-N$ stereogenic axis have been reported:⁴ barbiturates are the most studied class of biologically active compounds,⁵ and lactams,⁶ pyrroles,⁷ indoles,⁸ imides,⁹ azalidine-4-ones,¹⁰ thiazolidine-2-thiones,¹¹ and xanthenes¹² are found to exhibit stereodynamic properties.

1-Aryl-2-iminoazacycloalkanes are expected to have the plane of the *ortho*-substituted phenyl ring significantly twisted with respect to the time-averaged plane of the five-, six-, and

seven-membered heterocyclic ring. The existence of such an $Ar-N$ stereogenic axis would originate, in principle, a pair of stereolabile enantiomeric forms when the rotation rate is rendered sufficiently slow in the nuclear magnetic resonance (NMR) time scale. The aim of this paper is a thorough investigation of the stereodynamic behavior of a new class of compounds having a $C_{aryl}-N$ stereogenic axis in a five-membered saturated ring,¹³ (1-arylpyrrolidin-2-imines **1–9** and their oxo-analogues **18–20** Scheme 1), and the evaluation of the steric effect of the *ortho*-aryl substituents. Moreover, the six- and seven-membered imino homologues (**10–13** and **14–17**, respectively) and their oxo-analogues **21–22** have been prepared to evaluate the effect of the ring size and of the exocyclic heteroatom on the *N*-aryl rotational barrier.

RESULTS AND DISCUSSION

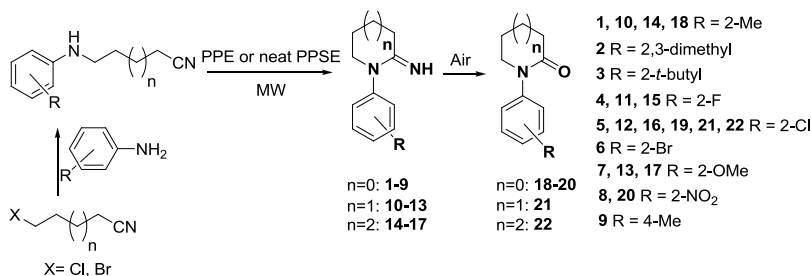
When an *ortho*-substituted aryl ring is bonded to pyrrolidin-2-imines (Scheme 1), the steric hindrance caused by the *ortho*-substituent forces the aryl ring to adopt a skewed conformation with respect to the almost planar heterocyclic ring, thus generating a stereogenic axis and a pair of conformational enantiomers when the rotational barrier is frozen; depending

Received: January 22, 2019

Accepted: February 19, 2019

Published: March 4, 2019

Scheme 1. Synthesis of Compounds 1–22



on the value of the rotational barrier, stereolabile enantiomers or atropisomers can be generated. In addition to the stereogenic axis, a second source of stereoisomerism could be anticipated because of the presence of the imine moiety that can have *E* or *Z* configuration.¹⁴ This conformational feature must be carefully considered because of the different steric hindrance exerted by the NH moiety in the *E* or *Z* stereoisomer on the *N*-aryl ring rotation. To evaluate the energy barriers for the *N*-aryl rotation, density functional theory (DFT) calculations were performed using the M06-2X functional and the 6-311+G(d,p) basis set. All the optimized structures were verified to be true ground states by frequency analysis, showing the absence of imaginary frequencies. For each *E/Z* stereoisomer, the optimized structures showed that the aryl ring was twisted with respect to the heterocyclic ring with $C_2-C_4-N-C_2$ dihedral angles (ϕ) of about 60° and 120° , yielding a total of four ground states (for compound 1, see Figure 1, top). The interconversion of the two conforma-

computational details for compounds 1–22 are reported in the Supporting Information). The higher values calculated of the *Z*-stereoisomer are due to the larger steric hindrance caused by the imine hydrogen in the transition state geometries.

The lowest energy transition state is that of the *E* stereoisomer with a dihedral angle ϕ close to 180° ; this geometry avoids the steric clash between the *ortho*-substituent of the aryl ring and the imine NH and simultaneously minimizes the steric interaction between the *ortho*-H and the NH. The calculated energy barriers range from 2.9 kcal mol⁻¹ for compound 4 (*o*-fluoro) up to 21.3 kcal mol⁻¹ for compound 3, bearing a *tert*-butyl substituent in the *ortho* position. These energy barriers can be conveniently observed by the variable-temperature NMR technique (D-NMR),¹⁵ thanks to the presence of enantiotopic groups such as the two hydrogens of CH₂, which turn into anisochronous signals when the aryl rotation becomes slow in the NMR time scale. An example of the dynamic NMR experiment is shown in Figure 2 for compound 1.

At ambient temperature, the enantiotopic CH₂ in position 5 shows a triplet signal because of the coupling with CH₂ in position 4. On lowering the temperature, the signal broadens and reaches the coalescence point at -64°C , yielding a diastereotopic ABX₂ system below -91°C . From the rate constants obtained by line shape simulations at different temperatures, the activation energy value of 10.2 ± 0.15 kcal mol⁻¹ was derived using the Eyring equation. As usually happens in conformational processes, the activation entropy was found to be negligible.¹⁵ The same approach was used for compounds 2–22, and the experimental and calculated values are reported in Table 1 (variable-temperature NMR spectra and line shape simulations are reported in the Supporting Information).¹⁶

In the case of compound 3, the calculated energy barrier (21.3 kcal mol⁻¹) is much higher than the other compounds and indeed the two diastereotopic 5-CH₂ signals do not show any sign of dynamic exchange up to $+120^\circ\text{C}$, where the product begins to decompose. Therefore, a kinetic study was performed using one-dimensional exchange spectroscopy NMR (1D-EXSY NMR)¹⁷ at $+105^\circ\text{C}$ and $+110^\circ\text{C}$ in dimethyl sulfoxide (DMSO-*d*₆). The saturation transfer due to aryl rotation increases on raising the mixing time. First-order kinetic analysis allowed to determine the rate constants, yielding a ΔG^\ddagger value of 22.0 kcal mol⁻¹, in very good agreement with the DFT-calculated data (Figures 3 and S21 in the Supporting Information).

On the other side, compound 4 has the lowest calculated energy barrier (2.9 kcal mol⁻¹). In this case, the spectra had to be recorded below -100°C using CDFCl₂ as the solvent (Figure 4). The dynamic phenomenon begins at -149°C ,

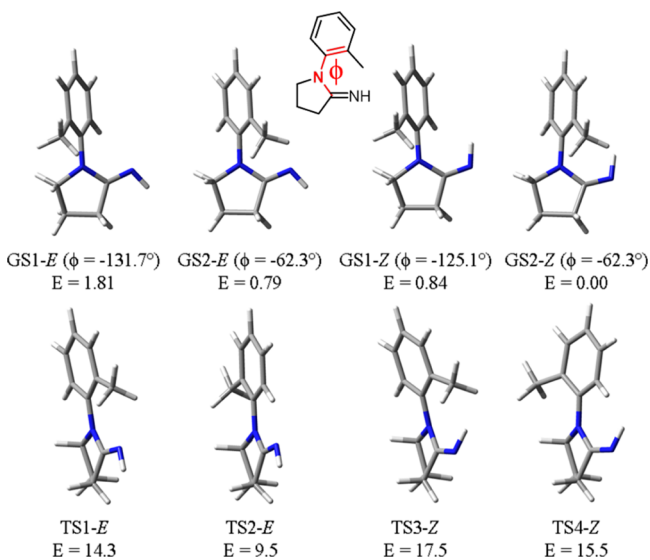


Figure 1. Top: Four ground states for compound 1 (in parentheses the value of the dihedral angle). Bottom: Four possible transition states for the *N*-aryl rotation (energies in the gas phase are reported in kcal mol⁻¹, relative to GS2-*Z*). Only the *M*-atropisomer is shown.

tional enantiomers can occur by the rotation of the aryl ring through two different transition states where the heterocyclic and the aromatic ring are almost coplanar, with dihedral angles ϕ close to 0° or 180° (TS1 and TS2 in Figure 1, bottom). In the case of compound 1, the calculated energy barriers were 9.5 and 14.3 kcal mol⁻¹ for the *E* stereoisomer, whereas they were calculated as 15.5 and 17.5 kcal mol⁻¹ in the *Z*-stereoisomer (all the DFT-calculated energies and the

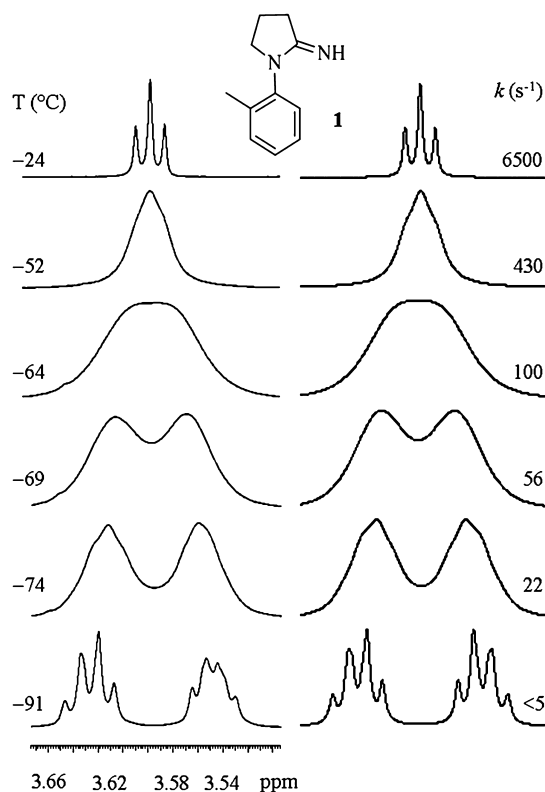


Figure 2. Left: ^1H NMR signal of CH_2 in position 5 of compound **1** at different temperatures (600 MHz in CD_2Cl_2). Right: Line shape simulations with the corresponding rate constants k in s^{-1} .

when the CH_2 signal broadens, reaches the coalescence at $-156\text{ }^\circ\text{C}$, and eventually splits showing four signals at $-165\text{ }^\circ\text{C}$. This occurrence implies that two diastereomeric conformations are present in a 73:27 ratio, both showing diastereotopic hydrogens. An additional dynamic process, ascribable to the E/Z conversion, has thus to be taken into account. The line shape simulations at different temperatures should be performed using three rate constants (N -aryl rotation in the E stereoisomer, N -aryl rotation in the Z stereoisomer, and E/Z interconversion), but good simulations were obtained by using only two kinetic constants. The first one accounts for the N -aryl rotation through the more stable transition state where the imine is the E configuration (Figure 4, AB peaks exchange). The second rate constant considers the exchange of E/Z stereoisomers (Figure 4, AC and BD peaks exchange), obtaining two energy barrier values of 5.3 ± 0.3 and $6.5 \pm 0.3\text{ kcal mol}^{-1}$, respectively. It must be underlined that the rotational rate constant for the aryl ring in the imine Z configuration is negligible because of the larger steric hindrance caused by the hydrogen in the planar TS. This occurrence implies that the rotational barrier in the stereoisomer is higher than the E/Z barrier, so the aryl rotation occurs only when the imine is in the E geometry.¹⁸

To confirm the assignment of this second dynamic process (i.e., E/Z interconversion of imine), we synthesized compound **9** with a p -methylphenyl substituent. This compound cannot have enantiomeric conformations because of local symmetry of the aryl ring, and any dynamic phenomenon has to be related to the E/Z conversion, which yields two diastereomeric conformations. Figure 5 shows the NMR spectra of compound **9**. At $-128\text{ }^\circ\text{C}$, the CH_3 signal broadens and eventually coalesces at $-133\text{ }^\circ\text{C}$. At $-149\text{ }^\circ\text{C}$, two distinct diastereomeric

singlet signals in a 70:30 ratio are visible. An energy barrier of $6.9 \pm 0.2\text{ kcal mol}^{-1}$ was derived from line shape simulations at different temperatures, a value identical to the higher barrier detected for compound **4**.

Using the B -value scale reported by Lunazzi et al.¹⁹ as an indicator to estimate the steric hindrance of various *ortho*-substituents, the very good correlation between the B -values and the experimental ΔG^\ddagger values of **1**, **3**–**8** (black rhombus in Figure 6, the table of values is reported in the Supporting Information) suggests that the magnitude of the enantiomerization barriers is mainly due to steric effects, as also forecasted by DFT calculations. It should be noted that the rotational barrier of the *o*-chloro compound is slightly smaller than that of the *o*-methyl, while the B -values series has opposite trend. However, this result is in agreement with a recent evaluation of the steric size of common substituents^{11b} and with the steric size scale proposed by Sternhell.²⁰


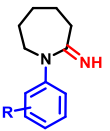
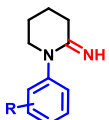
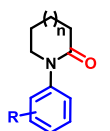
Six- and Seven-Membered Amidines. Switching from five-membered rings to the six-membered analogues, the energy barriers increase by about 5 kcal mol^{-1} (see Tables 1 and S6 and Figure S22 in the Supporting Information). This effect was previously observed for the rotational barriers of N -aryl five- and six-membered heterocyclic amidines (imidazolines and tetrahydropyrimidines, respectively).²¹ For 2-iminoazaheterocycles, the higher experimental value of six-membered derivatives is most probably the result of two opposite factors. On the one side, the higher steric constraints imposed in the TS by the different ring size should raise the rotational barrier because of the higher steric hindrance of the imino group in the TS. This effect is due to the geometry of the six-membered ring that moves the $=\text{NH}$ moiety toward the aryl ring in the TS geometry. On the other side, the higher flexibility of the six-membered ring allows the N -aryl group displacement in a pseudo-equatorial position, where the steric hindrance of the exocyclic imino moiety is reduced. This preference is well reproduced by DFT calculations on compound **11** (Figure S23 of the Supporting Information). The global minimum (GS4-Z in Figure S23) has the aryl ring in a pseudo-equatorial disposition, while the threshold transition state corresponds to the rotation of the *o*-fluorophenyl in a pseudo-axial disposition and with the fluorine on the $\text{C}=\text{NH}$ side (TS3-Z in Figure S23 of the Supporting Information).

In the case of the seven-membered ring, the increased flexibility of the ring compensates the higher steric hindrance on the TS and the energy barriers are similar to the six-membered rings. However, the larger size of the ring combined with the planarity of the imino portion makes the system to behave similar to a cyclohexane, with the $\text{N}-\text{C}_1$ moiety replacing a single carbon of cyclohexane.²²

The N -aryl ring can arrange itself onto a pseudo-equatorial or pseudo-axial position, and both conformations have similar energies (GS5-in and GS7-out, Figure 7).

In the case of compound **15** (Figure S11 in the Supporting Information), the triplet of the CH_2 signal splits into two diastereotopic signals below $-62\text{ }^\circ\text{C}$ and splits again into four signals on further lowering the temperature below $-75\text{ }^\circ\text{C}$. This behavior can be rationalized by considering the simultaneous freezing of the aryl rotation and the ring inversion, yielding two conformational diastereoisomers in a $\approx 50:50$ ratio, each one showing diastereotopic hydrogens for CH_2 (the E/Z interconversion takes place at much lower temperatures and cannot be responsible for the observed

Table 1. Experimental and Calculated Rotational Barriers for Compounds 1–22

Compound	R	DNMR $\Delta G^{\ddagger}_{\text{Exp.}}$	DFT $\Delta E^{\ddagger}_{\text{Calc.}}$	Compound	R	DNMR $\Delta G^{\ddagger}_{\text{Exp.}}$	DFT $\Delta E^{\ddagger}_{\text{Calc.}}$ ^g			
	1	CH ₃	10.2 ^a	9.5		14	CH ₃	15.9 ^d	16.8	
	2	2,3-diCH ₃	13.4 ^a	12.5		15	F	11.1 ^e	8.0	
	3	<i>t</i> -Bu	22.0 ^b	21.3		16	Cl	14.9 ^e	13.1	
	4	F	5.3 ^c	2.9		17	OCH ₃	12.8 ^d	11.4	
	5	Cl	9.9 ^e	7.5		n=0	18	CH ₃	9.4 ^a	8.4
	6	Br	10.5 ^a	8.7		n=0	19	Cl	9.3 ^c	6.6
	7	OCH ₃	8.6 ^c	5.6		n=0	20	NO ₂	8.6 ^c	6.6
	8	NO ₂	8.6 ^c	7.5		n=1	21	Cl	16.8 ^d	18.3
	9	<i>p</i> -CH ₃	6.9 ^{c,f}			n=2	22	Cl	16.7 ^d	13.9
	10	CH ₃	16.4 ^d	14.8		21	Cl	16.8 ^d	18.3	
	11	F	11.1 ^a	9.4		22	Cl	16.7 ^d	13.9	
	12	Cl	14.8 ^d	13.2						
	13	OCH ₃	13.0 ^d	11.5						

^aCalculations were performed at the M06-2X/6-311+G(d,p) level. Energy values are reported in kcal mol⁻¹. ^bCD₂Cl₂. ^cFrom 1D-EXSY analysis in toluene-*d*₆. ^dCDCl₂. ^eDMF-*d*₆. ^fDMSO-*d*₆. ^gBarrier of *E/Z* interconversion.

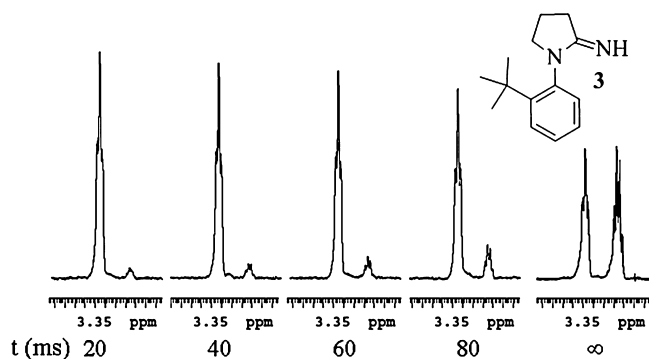


Figure 3. Kinetic study by 1D EXSY NMR of compound 3 (600 MHz in DMSO-*d*₆). Spectra are relative to the CH₂ signals in position 5 at +110 °C.

spectra). The two dynamic processes have similar energies (9.5 ± 0.2 and 11.1 ± 0.2 kcal mol⁻¹, respectively). Compound 16 (aryl = *o*-chloro) was prepared to obtain information on which of the two barriers is due to the rotation of the aryl and which one is related to the ring inversion. In compound 16, the aryl rotational barrier is much higher, and the ambient temperature spectrum shows diastereotopic signals for CH₂ (Figure S12 in the Supporting Information). On lowering the temperature, each diastereotopic signal broadens again and splits into two sets of diastereotopic signals below -70 °C, with a diastereomeric ratio of 61:39 (Figure S19 in the Supporting Information). This dynamic process must be assigned to the ring inversion, and the different diastereotopic ratio is a

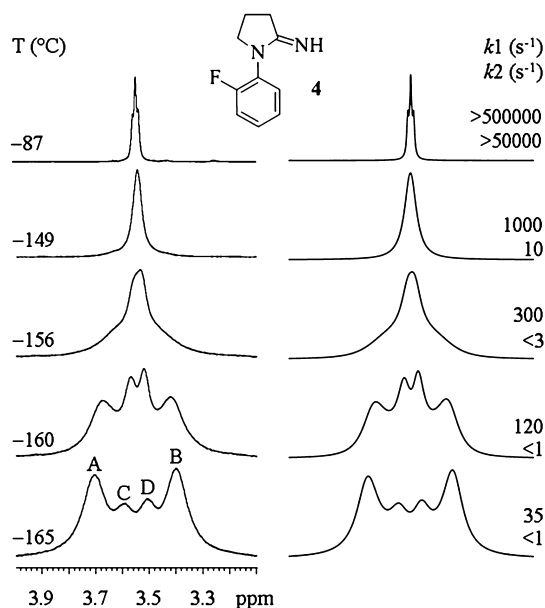


Figure 4. Left: ¹H NMR signal of CH₂ in position 5 of compound 4 at different temperatures (600 MHz in CDCl₂). Right: Line shape simulations with the corresponding rate constants *k*.

consequence of the higher steric hindrance exerted by chlorine with respect to fluorine. The experimental energy barrier was 9.5 ± 0.2 kcal mol⁻¹, in agreement to the smallest barrier observed for compound 15. The higher barrier observed for 15

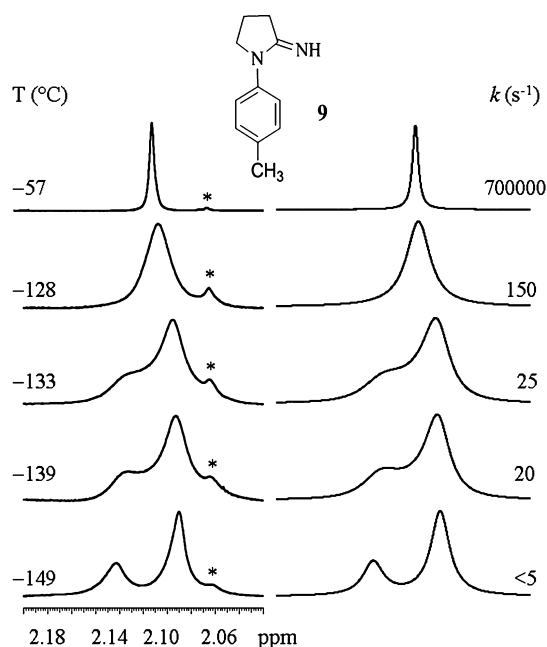


Figure 5. Left: ^1H NMR signal of the *p*- CH_3 signal of compound **9** at different temperatures (600 MHz in CDFCl_2). Right: Line shape simulations with the corresponding rate constants k . The line marked with the asterisk is an impurity.

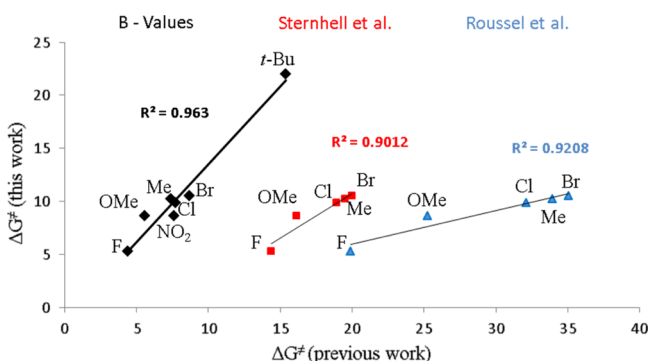


Figure 6. Experimental barriers determined for compounds **1**, **3**–**8** (y -axis), vs the values derived from three steric scales (x -axis). All the values are in kcal mol^{-1} .

($11.1 \text{ kcal mol}^{-1}$) has therefore to be assigned to the *o*-fluorophenyl rotation.

Carbonyl Compounds. As a last structural change, we prepared some carbonyl analogues (compounds **18**–**22**) to investigate the effects of the exocyclic heteroatom on the rotational barrier. From a theoretical point of view, the steric size of the carbonyl should be very similar to that of the *E*-stereoisomer of the imine. In the case of the five-membered rings (compounds **18**–**20**), the aryl rotational barriers are indeed very close to the corresponding imino compounds ($\text{R} = \text{Me}$, Cl , and NO_2), with differences lying just above the experimental error ($\pm 0.2 \text{ kcal/mol}$). On the contrary, in the case of the six- and seven-membered rings (compounds **21** and **22**, respectively), the rotational energy difference is about 2 kcal mol^{-1} higher than the imino compounds.

DFT calculations suggest that the geometry of the threshold TS (Figure S24 middle in the Supporting Information) in compound **21** is higher in energy and different in geometry with respect to the TS of compound **12**. In compound **21**, the

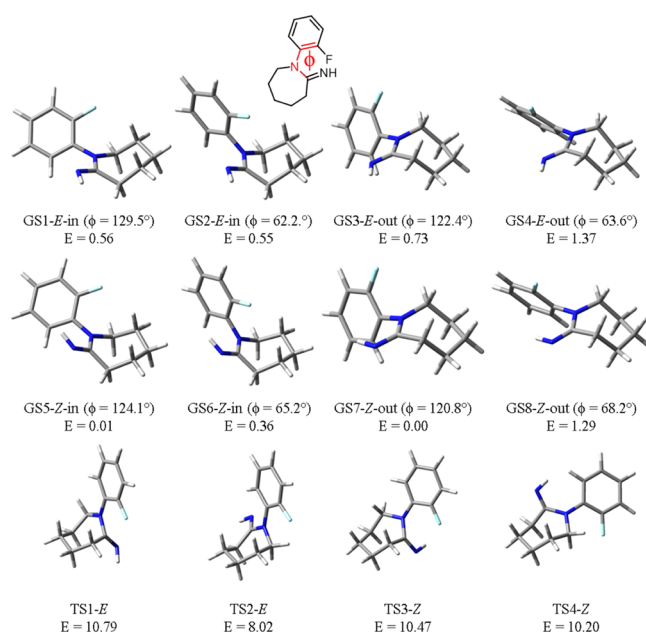


Figure 7. Compound **15** (in parentheses the value of the dihedral angle). Top: Four ground states of the *E* stereoisomer. Middle: Four ground states of the stereoisomer. Bottom: Four possible transition states for the *N*-aryl rotation (energies are reported in kcal mol^{-1} , relative to *GS7-out*). Only the *P*-conformations are shown.

o-chlorine atom is located over CH_2 in position 6 of the ring, and the two rings are almost coplanar. In compound **12**, the aryl ring is in a pseudo-axial position and the chlorine is on the side of the $\text{C}=\text{NH}$ moiety. The difference is due to the lower double-bond character of the amidine moiety with respect to the amide. This difference is confirmed by the observation of a lower $\text{C}-\text{N}$ rotational barrier in *N,N*-dimethylacetimidine with respect to *N,N*-dimethylacetamide.²³ The same effect can be invoked to explain the larger barrier of **22** with respect to **16** (Figure S24 in the Supporting Information). On the contrary, the smaller five-membered ring (e.g., compound **5** vs **19**) is more rigid and does not allow the aryl ring to bend out of the ring plane, thus the steric effect of the imino is similar to that of the carbonyl. DFT calculations confirmed that the geometries of both TS have the chlorine close to CH_2 in position 5 (Figure S24 in the Supporting Information). As observed for compound **16**, the low-temperature NMR spectra of compound **22** showed the presence of two diastereomeric conformations because of the ring inversion, with an energy barrier at the coalescence point of $9.7 \pm 0.2 \text{ kcal mol}^{-1}$, very similar to that observed for compound **16**.

CONCLUSIONS

We investigated the conformational dynamics of 1-aryl-2-iminoazacycloalkanes on increasing the ring size from five to seven members. The *N*-aryl rotational barrier was found to be driven by the steric size of the *ortho* substituent, and the barrier increases by about 5 kcal mol^{-1} when changing the ring size from five to six and seven members. The *E/Z* interconversion barrier of the imino moiety was measured as $6.9 \text{ kcal mol}^{-1}$ in compound **4**. Two conformational diastereoisomers, generated by ring inversion, were observed in the case of the seven-membered rings, with an energy barrier of $9.5 \text{ kcal mol}^{-1}$. A comparison with some carbonyl analogues showed very similar

N-aryl rotational barriers for the five-membered rings and slightly higher barriers for the larger rings.

■ EXPERIMENTAL SECTION

Spectroscopic Data. NMR spectra were recorded using a spectrometer operating at a field of 14.4 T (600 MHz for ^1H , 150.8 for ^{13}C). Chemical shifts are reported in ppm (δ) relative to tetramethylsilane as an internal standard. D_2O was employed to confirm exchangeable protons (ex). Splitting multiplicities are reported as singlet (s), broad signal (bs), doublet (d), double doublet (dd), triplet (t), quartet (q), heptet (h), and multiplet (m). The assignment of the ^{13}C signals was obtained by means of DEPT, gs-HSQC, and gs-HMBC spectra. The 150.8 MHz ^{13}C spectra were acquired under proton decoupling conditions with a 36 000 Hz spectral width, 5.5 μs (60° tip angle) pulse width, 1 s acquisition time, and 9 s delay time. The long relaxation time was needed to observe some quaternary carbons of the heterocycle. A line broadening function of 1–2 Hz was applied before the Fourier transformation. 1D-EXSY spectra were obtained at 600 MHz using the DPGFSE sequence²⁴ and a 50 Hz wide selective pulse with a R-SNOB shape.²⁵ High-resolution mass spectrometry (HRMS) was performed with an ESI-QTOF spectrometer. Reagents, solvents, and starting materials were purchased from standard sources and purified according to literature procedures. Melting points were determined with a Büchi capillary apparatus and are uncorrected. Variable-temperature NMR spectra were recorded as previously reported.²⁶ The rate constants were derived from line shape simulations (QCPE DNMR6 program),²⁷ and the free energies of activation (ΔG^\ddagger) were obtained by means of the Eyring equation. Within the experimental uncertainty, the latter values were found essentially invariant in the examined temperature range, thus implying an almost negligible activation entropy ΔS^\ddagger .¹⁵

Calculations. The ground-state and transition-state geometries were obtained using the Gaussian 09 rev D.01 series of programs,²⁸ with standard optimization parameters. The calculations employed the M06-2X hybrid-DFT functional²⁹ and the 6-311+G(d,p) basis set. Vibrational analysis was performed to validate the ground states (zero imaginary frequencies) and the transition states (one imaginary frequency). Visual inspection of the corresponding normal mode³⁰ confirmed the identification of the correct transition states.

Materials. Compounds (1, 5, 7, 9, 10–12, 14–15, 27, 29, 33, 34, 36, 37),³ 18,³¹ (19, 21),³² 22,³³ (23, 31, 32)³⁴ were described in the literature.

General Procedure for the Synthesis of 1-N-Aryl-2-iminopyrrolidines 1–9.³ A mixture of the corresponding 4-arylamino butyronitriles (0.5 mmol) and a chloroform solution of PPE (4 mL) was reacted in a microwave reactor (Monowave 300, Anton Paar) at 100 °C for 5 min for compounds 1 and 4–9 or 30 min for compounds 2 and 3. After reaching room temperature, the resulting solution was extracted with water (5 \times 8 mL). The aqueous phases were pooled, filtered, and made alkaline in an ice bath, and the mixture was extracted with dichloromethane (3 \times 40 mL). The organic layer was washed with water (5 mL), dried over sodium sulfate, and filtered. The solvent was removed in vacuo. The crude products were purified by column chromatography [Silica gel 60, dichloromethane (DCM)/methanol 30:1, DCM/isopropylamine 30:1].

General Procedure for the Synthesis of 1-N-Aryl-2-iminopyrrolidines 10–13 and 1-N-Aryl-2-iminoazepanes 14–17.³ A mixture of the corresponding compound 5-arylaminovaleronitriles or 6-arylamino hexanenitriles (0.5 mmol) and neat PPSE (3 g) was reacted in the microwave reactor (Monowave 300, Anton Paar) at 150 °C for 30 min for compounds 10–13 and at 200 °C for 30 min for compounds 14–17. After reaching room temperature, the resulting oil was treated with dichloromethane (25 mL) and 10% aqueous NaOH (15 mL). The aqueous phase was extracted with dichloromethane (2 \times 25 mL). The organic phases were pooled, washed with water (5 mL), filtered, dried over sodium sulfate, and filtered. The solvent was removed in vacuo. The crude products were purified by column chromatography (silica gel 60; DCM/methanol 30:1, DCM/isopropylamine 30:1).

General Procedure for the Synthesis of 1-N-Aryl-2-pyrrolidinones 18–20. An aliquot (0.5 mmol) of the compounds 1, 5, 8, 12, or 16 is kept at room temperature in an open vessel without any solvent. After 48 h, one of the hydrolysis products, 1-aryl-2-pyrrolidinone, is obtained. The product is purified by column chromatography (silica gel 60; DCM/methanol 50:1).

General Procedure for the Synthesis of 4-Arylamino butyronitriles 23–31, 5-Arylaminovaleronitriles 32–35, and 6-Arylamino hexanenitriles 36–39.^{3,33} A solution of the corresponding precursor (4-chlorobutyronitrile for compounds 23–31, 5-chlorovaleronitrile for compounds 32–35, and 6-bromohexanenitrile for compounds 36–39) (2.5 mmol) in dimethylformamide or dimethylsulfoxide (for compound 30) (1 mL) was added during 1.5 h to a mixture of the arylamine (2.5 mmol), Cs_2CO_3 (2.5 mmol), and KI (5 mmol) in dimethylformamide or dimethylsulfoxide (for compound 30) (2.5 mL). The mixture was stirred at 110 °C for 8 h (compounds 24, 26–29, 32–35), at 75 °C for 8 h (compounds 23, 31), at 145 °C for 7 h (compounds 25, 30), or at 70 °C for 6 h (compounds 36–39). After completion of the reaction, as indicated by thin-layer chromatography, the mixture was treated with ethyl ether (50 mL) and water (10 mL). The aqueous phase was separated and extracted with ethyl ether (30 mL). The combined organic layers were dried over anhydrous sodium sulfate and filtered. The solvent was evaporated in vacuo. The crude product was purified by column chromatography (silica gel 60; DCM/hexane 8:2).

1-(2,3-Dimethylphenyl)-2-iminopyrrolidine (2). Yellow oil (60% yield). ^1H NMR (600 MHz, CDCl_3): δ 2.07 (s, 3H), 2.09–2.14 (m, 2H), 2.29 (s, 3H), 2.70 (t, $J = 7.9$ Hz, 2H), 3.62–3.66 (m, 2H), 4.40 (bs, ex, 1H), 7.00 (d, $J = 7.0$ Hz, 1H), 7.10–7.14 (m, 2H). ^{13}C NMR (150 MHz, CDCl_3): δ 13.9, 20.3, 20.6, 31.9, 53.0, 125.1, 126.6, 129.2, 135.1, 138.0, 138.5, 167.7. HRMS (ESI-QTOF) m/z : calcd for $\text{C}_{12}\text{H}_{17}\text{N}_2$, 189.13862; found, 189.13907.

1-(*o*-tert-Butylphenyl)-2-iminopyrrolidine (3). White solid (83% yield), mp: 59–61 °C. ^1H NMR (600 MHz, CDCl_3): δ 1.37 (s, 9H), 2.08–2.14 (m, 2H), 2.66–2.76 (m, 2H), 3.56–3.61 (m, 1H), 3.67–3.71 (m, 1H), 4.83 (bs, ex, 1H), 7.02–7.04 (m, 1H), 7.27–7.32 (m, 2H), 7.51–7.52 (m, 1H). ^{13}C NMR (150 MHz, CDCl_3): δ 20.2, 31.2, 31.6, 35.3, 55.5, 127.9, 128.0, 128.2, 130.5, 139.1, 149.8, 170.2. HRMS (ESI-QTOF) m/z : calcd for $\text{C}_{14}\text{H}_{21}\text{N}_2$, 217.16993; found, 217.17040.

1-(*o*-Fluorophenyl)-2-iminopyrrolidine (4). Yellow oil (83% yield). ^1H NMR (600 MHz, CD_3CN): δ 2.03–2.08

(m, 2H), 2.57 (t, $J = 7.8$ Hz, 2H), 3.70 (td, $J = 6.7, 0.6$ Hz, 2H), 7.16–7.21 (m, 2H), 7.24–7.27 (m, 1H), 7.45 (td, $J = 8.1, 1.9$ Hz, 1H). ^{13}C NMR (150 MHz, CD_3CN): δ 22.0, 33.2, 53.4, 117.8 (d, $J_{\text{C-F}} = 20.4$ Hz), 126.0 (d, $J_{\text{C-F}} = 3.3$ Hz), 128.9 (d, $J_{\text{C-F}} = 8.3$ Hz), 129.8 (d, $J_{\text{C-F}} = 2.8$ Hz), 130.0 (d, $J_{\text{C-F}} = 11.6$ Hz), 159.1 (d, $J_{\text{C-F}} = 247.9$ Hz), 168.8. HRMS (ESI-QTOF) m/z : calcd for $\text{C}_{10}\text{H}_{12}\text{FN}_2$, 179.09790; found, 179.09725.

1-(*o*-Bromophenyl)-2-iminopyrrolidine (6). Yellow oil (57% yield). ^1H NMR (600 MHz, CD_2Cl_2): δ 2.11–2.16 (m, 2H), 2.65 (t, $J = 7.9$ Hz, 2H), 3.70 (t, $J = 6.8$ Hz, 2H), 5.12 (bs, ex, 1H), 7.19–7.22 (m, 1H), 7.37–7.40 (m, 1H), 7.67 (dd, $J = 8.0, 1.4$ Hz, 1H). ^{13}C NMR (150 MHz, CD_2Cl_2): δ 21.5, 32.6, 52.9, 123.8, 129.3, 129.7, 131.0, 134.3, 139.8, 168.1. HRMS (ESI-QTOF) m/z : calcd for $\text{C}_{10}\text{H}_{12}\text{BrN}_2$, 239.01784; found, 239.01846.

1-(*o*-Nitrophenyl)-2-iminopyrrolidine (8). Yellow oil (22% yield). ^1H NMR (600 MHz, CD_3CN): δ 2.06–2.11 (m, 2H), 2.53 (t, $J = 7.8$ Hz, 2H), 3.82 (t, $J = 6.8$ Hz, 2H), 7.34–7.37 (m, 1H), 7.45 (dd, $J = 8.1, 1.3$ Hz, 1H), 7.65–7.68 (m, 1H), 7.86 (dd, $J = 7.9, 1.5$ Hz, 1H). ^{13}C NMR (150 MHz, CD_3CN): δ 22.0, 33.6, 53.1, 128.2, 127.2, 126.3, 137.7, 135.9, 135.0, 168.6. HRMS (ESI-QTOF) m/z : calcd for $\text{C}_{10}\text{H}_{11}\text{N}_3\text{O}_2$, 205.08513; found, 205.08512.

1-(*o*-Methoxyphenyl)-2-iminopiperidine (13). Brown oil (75% yield). ^1H NMR (600 MHz, CD_3CN): δ 1.79–1.82 (m, 2H), 1.83–1.87 (m, 2H), 2.46 (t, $J = 6.6$ Hz, 2H), 3.36 (bs, 2H), 3.79 (s, 3H), 6.98 (t, $J = 7.6$ Hz, 1H), 7.07 (d, $J = 8.2$ Hz, 1H), 7.14 (dd, $J = 7.6, 1.5$ Hz, 1H), 7.28–7.31 (m, 1H). ^{13}C NMR (150 MHz, CDCl_3): δ 21.5, 23.9, 31.7, 50.3, 55.6, 112.5, 121.4, 128.8, 129.9, 131.7, 155.7, 163.5. HRMS (ESI-QTOF) m/z : calcd for $\text{C}_{12}\text{H}_{17}\text{N}_2\text{O}$, 205.13354; found, 205.13421.

1-(*o*-Chlorophenyl)-2-iminoazepane (16). Brown oil (17% yield). ^1H NMR (500 MHz, CDCl_3): δ 1.65–2.07 (m, 6H), 2.71–2.77 (m, 2H), 3.44–3.57 (m, 1H), 3.67–3.79 (m, 1H), 4.40 (bs, ex, 1H), 7.25–7.29 (m, 2H), 7.32–7.35 (m, 1H), 7.50–7.52 (m, 1H). ^{13}C NMR (125 MHz, CDCl_3): δ 25.5, 29.4, 29.9, 37.1, 53.3, 128.3, 128.6, 130.4, 130.8, 133.1, 142.4, 168.8. HRMS (ESI-QTOF) m/z : calcd for $\text{C}_{12}\text{H}_{16}\text{ClN}_2$, 223.09965; found, 223.09920.

1-(*o*-Methoxyphenyl)-2-iminoazepane (17). Brown oil (40% yield). ^1H NMR (600 MHz, CDCl_3): δ 1.62–1.84 (m, 6H), 2.65–2.68 (m, 2H), 3.49–3.55 (m, 1H), 3.79 (s, 3H), 4.08 (bs, 2H), 6.92–6.97 (m, 2H), 7.11–7.14 (m, 1H), 7.22–7.28 (m, 1H). ^{13}C NMR (150 MHz, CDCl_3): δ 25.7, 29.2, 29.9, 36.6, 53.3, 55.6, 112.5, 121.2, 128.5, 129.9, 133.1, 155.4, 169.3. HRMS (ESI-QTOF) m/z : calcd for $\text{C}_{13}\text{H}_{19}\text{N}_2\text{O}$, 219.14919; found, 219.14844.

1-(*o*-Nitrophenyl)-2-pyrrolidinone (20). Yellow oil (62% yield). ^1H NMR (600 MHz, CDCl_3): δ 2.25–2.30 (m, 2H), 2.55 (t, $J = 8.1$ Hz, 2H), 3.89 (t, $J = 7.0$ Hz, 2H), 7.36 (dd, $J = 7.9, 1.2$ Hz, 1H), 7.41–7.44 (m, 1H), 7.64 (td, $J = 7.9, 1.5$ Hz, 1H), 7.98 (dd, $J = 8.2, 1.5$ Hz, 1H). ^{13}C NMR (150 MHz, CDCl_3): δ 19.1, 31.2, 50.2, 125.6, 127.5, 127.6, 132.4, 133.7, 145.8, 174.9. HRMS (ESI-QTOF) m/z : calcd for $\text{C}_{10}\text{H}_{11}\text{N}_2\text{O}_3$, 207.07642; found, 207.07645.

4-(2,3-Dimethylphenylamino)butyronitrile (24). White solid (72% yield), mp: 82–84 °C. ^1H NMR (500 MHz, CDCl_3): δ 1.99–2.05 (m, 2H), 2.08 (s, 3H), 2.31 (s, 3H), 2.50 (t, $J = 7.1$ Hz, 2H), 3.37 (t, $J = 6.6$ Hz, 2H), 3.60 (bs, ex, 1H), 6.54 (d, $J = 8.0$ Hz, 1H), 6.66 (d, $J = 7.6$ Hz, 1H), 7.04–7.08 (m, 1H). ^{13}C NMR (125 MHz, CDCl_3): δ 14.3, 14.8, 20.6, 25.1, 42.4, 107.8, 119.4, 119.8, 120.6, 126.1, 136.7, 145.2.

HRMS (ESI-QTOF) m/z : calcd for $\text{C}_{12}\text{H}_{17}\text{N}_2$, 189.13862; found, 189.13909.

4-(*o*-tert-Butylphenylamino)butyronitrile (25). Yellow oil (70% yield). ^1H NMR (300 MHz, CDCl_3): δ 1.45 (s, 9H), 2.01–2.10 (m, 2H), 2.51 (t, $J = 7.1$ Hz, 2H), 3.41 (bs, 2H), 3.94 (bs, ex, 1H), 6.70 (d, $J = 8.1$ Hz, 1H), 6.74–6.79 (m, 1H), 7.14–7.19 (m, 1H), 7.30 (d, $J = 7.9$ Hz, 1H). ^{13}C NMR (75 MHz, CDCl_3): δ 14.9, 25.2, 29.9, 34.1, 42.6, 111.7, 117.6, 119.3, 126.4, 127.1, 133.6, 145.5. HRMS (ESI-QTOF) m/z : calcd for $\text{C}_{14}\text{H}_{21}\text{N}_2$, 217.16993; found, 217.17026.

4-(*o*-Fluorophenylamino)butyronitrile (26). Brown oil (60% yield). ^1H NMR (300 MHz, CDCl_3): δ 1.93–2.02 (m, 2H), 2.48 (t, $J = 7.1$ Hz, 2H), 3.30–3.36 (m, 2H), 3.97 (bs, ex, 1H), 6.62–6.74 (m, 2H), 6.95–7.04 (m, 2H). ^{13}C NMR (75 MHz, CDCl_3): δ 14.6, 25.1, 41.8, 111.9 (d, $J_{\text{C-F}} = 3.3$ Hz), 114.5 (d, $J_{\text{C-F}} = 18.2$ Hz), 117.1 (d, $J = 7.2$ Hz), 119.2, 124.6 (d, $J_{\text{C-F}} = 3.3$ Hz), 135.9 (d, $J_{\text{C-F}} = 11.6$ Hz), 151.5 (d, $J_{\text{C-F}} = 238.3$ Hz). HRMS (ESI-QTOF) m/z : calcd for $\text{C}_{10}\text{H}_{12}\text{FN}_2$, 179.09790; found, 179.09715.

4-(*o*-Bromophenylamino)butyronitrile (28). Yellow oil (54% yield). ^1H NMR (500 MHz, CDCl_3): δ 1.98–2.03 (m, 2H), 2.48 (t, $J = 7.1$ Hz, 2H), 3.87 (t, $J = 6.6$ Hz, 2H), 4.44 (bs, ex, 1H), 6.60–6.63 (m, 1H), 6.66 (dd, $J = 8.2, 1.4$ Hz, 1H), 7.18–7.21 (m, 1H), 7.44 (dd, $J = 7.9, 1.5$ Hz, 1H). ^{13}C NMR (125 MHz, CDCl_3): δ 14.7, 24.9, 42.1, 110.0, 111.3, 118.4, 119.1, 128.5, 132.6, 144.1. HRMS (ESI-QTOF) m/z : calcd for $\text{C}_{10}\text{H}_{12}\text{BrN}_2$, 239.01784; found, 239.01846.

4-(*o*-Nitrophenylamino)butyronitrile (30). Yellow oil (7% yield). ^1H NMR (500 MHz, CDCl_3): δ 2.07–2.12 (m, 2H), 2.53 (t, $J = 7.0$ Hz, 2H), 3.50–3.54 (m, 2H), 6.71 (ddd, $J = 8.6, 7.0, 1.4$ Hz, 1H), 6.87–6.89 (m, 1H), 7.48 (ddd, $J = 8.6, 7.0, 1.5$ Hz, 1H), 8.19 (dd, $J = 8.6, 1.5$ Hz, 1H). ^{13}C NMR (125 MHz, CDCl_3): δ 14.9, 24.9, 41.2, 113.4, 116.0, 118.6, 127.1, 130.9, 136.5, 144.9. HRMS (ESI-QTOF) m/z : calcd for $\text{C}_{10}\text{H}_{12}\text{N}_3\text{O}_2$, 206.09240; found, 206.09227.

5-(*o*-Methoxyphenylamino)valeronitrile (35). Yellow oil (75% yield). ^1H NMR (500 MHz, CDCl_3): δ 1.78–1.83 (m, 4H), 2.37–2.41 (m, 2H), 3.18–3.21 (m, 2H), 3.86 (s, 3H), 6.62 (dd, $J = 7.8, 1.5$ Hz, 1H), 6.68–6.71 (m, 1H), 6.79 (dd, $J = 8.0, 1.4$ Hz, 1H), 6.87–6.90 (m, 1H). ^{13}C NMR (125 MHz, CDCl_3): δ 16.9, 23.06, 28.4, 42.6, 55.3, 109.4, 109.7, 116.6, 119.4, 121.2, 137.7, 146.7. HRMS (ESI-QTOF) m/z : calcd for $\text{C}_{12}\text{H}_{17}\text{N}_2\text{O}$, 205.13354; found, 205.13404.

6-(*o*-Chlorophenylamino)hexanenitrile (38). Yellow oil (87% yield). ^1H NMR (500 MHz, CDCl_3): δ 1.58–1.65 (m, 2H), 1.71–1.78 (m, 4H), 2.40 (t, $J = 7.1$ Hz, 2H), 3.22 (t, $J = 7.0$ Hz, 2H), 4.45 (bs, ex, 1H), 6.65–6.69 (m, 2H), 7.17 (ddd, $J = 8.1, 7.3, 1.5$ Hz, 1H), 7.28 (dd, $J = 7.8, 1.4$ Hz, 1H). ^{13}C NMR (125 MHz, CDCl_3): δ 17.1, 25.2, 26.2, 28.5, 43.3, 111.2, 117.3, 119.1, 119.5, 127.8, 129.1, 143.7. HRMS (ESI-QTOF) m/z : calcd for $\text{C}_{12}\text{H}_{16}\text{ClN}_2$, 223.09965; found, 223.09926.

6-(*o*-Methoxyphenylamino)hexanenitrile (39). Yellow oil (74% yield). ^1H NMR (500 MHz, CDCl_3): δ 1.55–1.62 (m, 2H), 1.67–1.75 (m, 4H), 2.36 (t, $J = 7.1$ Hz, 2H), 3.16 (t, $J = 7.0$ Hz, 2H), 3.85 (s, 3H), 6.62 (dd, $J = 7.8, 1.4$ Hz, 1H), 6.66–6.70 (m, 1H), 6.78 (dd, $J = 7.9, 1.3$ Hz, 1H), 6.86–6.89 (m, 1H). ^{13}C NMR (125 MHz, CDCl_3): δ 17.1, 25.2, 26.3, 28.7, 43.3, 55.3, 109.4, 109.9, 116.5, 119.6, 121.2, 137.9, 146.8. HRMS (ESI-QTOF) m/z : calcd for $\text{C}_{13}\text{H}_{19}\text{N}_2\text{O}$, 219.14919; found, 219.14939.

■ ASSOCIATED CONTENT

Supporting Information

The Supporting Information is available free of charge on the ACS Publications website at DOI: 10.1021/acsomega.9b00192.

Dynamic NMR data for compounds **2**, **5–8**, **10–22**; kinetic study for compound **3**; DFT calculations for compounds **1–22**; and copies of ^1H and ^{13}C NMR spectra of compounds **1–22**, **24–26**, **28**, **30**, **35**, **38–39** (PDF)

■ AUTHOR INFORMATION

Corresponding Authors

*E-mail: lorelli@ffyb.uba.ar (L.R.O.).

*E-mail: michele.mancinelli@unibo.it (M.M.).

ORCID

Andrea Mazzanti: 0000-0003-1819-8863

Liliana R. Orelli: 0000-0001-7654-7211

Michele Mancinelli: 0000-0002-8499-5265

Notes

The authors declare no competing financial interest.

■ ACKNOWLEDGMENTS

Financial contribution was received by A.M. and M.M. from the University of Bologna (RFO funds 2015 and 2016) and by L.R.O. from the University of Buenos Aires (grant 20020130100466BA, 2014–2017). ALCHEMY Fine Chemicals & Research (Bologna, www.alchemy.it) is gratefully acknowledged for a generous gift of chemicals.

■ REFERENCES

- (1) (a) Hussain, A.; Yousuf, S. K.; Mukherjee, D. Importance and Synthesis of Benzannulated Medium-sized and Macrocyclic Rings (BMRs). *RSC Adv.* **2014**, *4*, 43241–43257. (b) Vitaku, E.; Smith, D. T.; Njardarson, J. T. Analysis of the Structural Diversity, Substitution Patterns, and Frequency of Nitrogen Heterocycles among U.S. FDA Approved Pharmaceuticals. *J. Med. Chem.* **2014**, *57*, 10257–10274.
- (2) Hagen, T. J.; Bergmanis, A. A.; Kramer, S. W.; Fok, K. F.; Schmelzer, A. E.; Pitzele, B. S.; Swenton, L.; Jerome, G. M.; Kornmeier, C. M.; Moore, W. M.; Branson, L. F.; Connor, J. R.; Manning, P. T.; Currie, M. G.; Hallinan, E. A. 2-Iminopyrrolidines as Potent and Selective Inhibitors of Human Inducible Nitric Oxide Synthase II. *J. Med. Chem.* **1998**, *41*, 3675–3683.
- (3) Diaz, J. E.; Mollo, M. C.; Orelli, L. R. Microwave-assisted Cyclizations Promoted by Polyphosphoric Acid Esters: a General Method for 1-Aryl-2-iminoazacycloalkanes. *Beilstein J. Org. Chem.* **2016**, *12*, 2026–2031.
- (4) Alkorta, I.; Elguero, J.; Roussel, C.; Vanthuyne, N.; Piras, P. Atropisomerism and Axial Chirality in Heteroaromatic Compounds. *Adv. Heterocycl. Chem.* **2012**, *105*, 1.
- (5) Oğuz, S. F.; Dogan, I. Determination of Energy Barriers and Racemization Mechanisms for Thermally Interconvertible Barbituric and Thiobarbituric Acid Enantiomers. *Tetrahedron: Asymmetry* **2003**, *14*, 1857–1864.
- (6) Kitagawa, O.; Fujita, M.; Kohriyama, M.; Hasegawa, H.; Taguchi, T. Stereoselective Synthesis of Diastereomeric Atropisomeric Lactam with Various Ring Sizes and Their Structural Characterization. *Tetrahedron Lett.* **2000**, *41*, 8539–8544.
- (7) Bock, L. H.; Adams, R. The stereochemistry of N-phenylpyrroles. The preparation and Resolution of N-2-Carboxyphenyl-2,5-dimethyl-3-carboxypyrrole. XIII. *J. Am. Chem. Soc.* **1931**, *53*, 374–376.
- (8) (a) Bringmann, G.; Tasler, S.; Endress, H.; Kraus, J.; Messer, K.; Wohlfarth, M.; Lobin, W. F. First Total Synthesis, Atropo-Enantiomer

Resolution, and Stereoanalysis of an Axially Chiral N,C-Coupled Biaryl Alkaloid. *J. Am. Chem. Soc.* **2001**, *123*, 2703–2711. (b) Kamikawa, K.; Kinoshita, S.; Furusyo, M.; Takemoto, S.; Matsuzaka, H.; Uemura, M. Stereoselective Synthesis of Both Enantiomers of N-Aryl Indoles with Axially Chiral N–C Bonds. *J. Org. Chem.* **2007**, *72*, 3394–3402.

(9) Shimizu, K. D.; Freyer, H. O.; Adams, R. D. Synthesis, Resolution and Structure of Axially Chiral Atropisomeric N-arylimides. *Tetrahedron Lett.* **2000**, *41*, 5431–5434.

(10) Yilmaz, E. M.; Doğan, I. Axially Chiral N-(*o*-aryl)-2-thioxo-oxazolidine-4-one and Rhodanine Derivatives: enantiomeric separation and determination of racemization barriers. *Tetrahedron: Asymmetry* **2008**, *19*, 2184–2191.

(11) (a) Ciogli, A.; Vivek Kumar, S.; Mancinelli, M.; Mazzanti, A.; Perumal, S.; Severi, C.; Villani, C. Atropisomerism in 3-arylthiazolidine-2-thiones. A combined Dynamic NMR and Dynamic HPLC study. *Org. Biomol. Chem.* **2016**, *14*, 11137–11147. (b) Belot, V.; Farran, D.; Jean, M.; Albalat, M.; Vanthuyne, N.; Roussel, C. Steric Scale of Common Substituents from Rotational Barriers of N-(*o*-Substituted aryl)thiazoline-2-thione Atropisomers. *J. Org. Chem.* **2017**, *82*, 10188–10200.

(12) Mancinelli, M.; Perticarari, S.; Prati, L.; Mazzanti, A. Conformational Analysis and Absolute Configuration of Axially Chiral 1-aryl and 1,3-bisaryl-xanthenes. *J. Org. Chem.* **2017**, *82*, 6874–6885.

(13) Bonne, D.; Rodriguez, J. A Bird's Eye View of Atropisomers Featuring a Five-Membered Ring. *Eur. J. Org. Chem.* **2018**, *2018*, 2417–2431.

(14) For a review on this subject, see: Jennings, W. B.; Wilson, V. E. In *Acyclic Organonitrogen Stereodynamics*; Lambert, J. B., Takeuchi, Y., Eds.; VCH Publishers: New York, 1991; Chapter 6, pp 155–243 and references cited therein.

(15) For a review see: Casarini, D.; Lunazzi, L.; Mazzanti, A. Recent Advances in Stereodynamics and Conformational Analysis by Dynamic NMR and Theoretical Calculations. *Eur. J. Org. Chem.* **2010**, *2010*, 2035–2056.

(16) The high temperature spectra were obtained in DMF-*d*7 or DMSO-*d*6. The use of a high-boiling chlorinated solvent similar to CD_2Cl_2 would have been preferable. However, we could not use 1,1,2,2-tetrachloroethane-*d*2 because at high temperatures the compounds react causing removal of DCl.

(17) 1D-EXSY were obtained by the DPFGE-NOE sequence using an array of short mixing times. See: Lunazzi, L.; Mancinelli, M.; Mazzanti, A. Stereodynamics and Conformational Chirality of the Atropisomers of Ditolyl Anthrones and Anthraquinone. *J. Org. Chem.* **2008**, *73*, 5354–5359.

(18) For a similar case see Casarini, D.; Lunazzi, L.; Mazzanti, A.; Foresti, E. Conformational Studies by Dynamic NMR. 64. Stereo-mutations of Atropisomers and of Conformational Enantiomers in Ethers of Hindered Naphthylcarbinols. *J. Org. Chem.* **1998**, *63*, 4746–4754.

(19) (a) Lunazzi, L.; Mancinelli, M.; Mazzanti, A.; Lepri, S.; Ruzziconi, R.; Schlosser, M. Rotational Barriers of Biphenyls Having Heavy Heteroatoms as ortho-Substituents: Experimental and Theoretical Determination of Steric Effects. *Org. Biomol. Chem.* **2012**, *10*, 1847–1855.

(20) Bott, G.; Field, L. D.; Sternhell, S. Steric Effects. A Study of a Rationally Designed System. *J. Am. Chem. Soc.* **1980**, *102*, 5618–5626.

(21) (a) Garcia, M. B.; Grilli, S.; Lunazzi, L.; Mazzanti, A.; Orelli, L. R. Conformational Studies by Dynamic NMR. 84.1 Structure, Conformation, and Stereodynamics of the Atropisomers of N-Aryl-tetrahydropyrimidines. *J. Org. Chem.* **2001**, *66*, 6679–6684. (b) Diaz, J. E.; Gruber, N.; Lunazzi, L.; Mazzanti, A.; Orelli, L. R. Conformation and stereodynamics of 1,2-diaryltetrahydropyrimidine and of its five- and seven-membered ring analogs. *Tetrahedron* **2011**, *67*, 9129–9133.

(22) Gruber, T.; Thompson, A. L.; Odell, B.; Bombicz, P.; Schofield, C. J. Conformational studies on Substituted ϵ -Caprolactams by X-ray

Crystallography and NMR Spectroscopy. *New J. Chem.* **2014**, *38*, 5905–5917.

(23) (a) Neuman, R. C.; Young, L. B. Hindered Rotation and Carbon-13-hydrogen Coupling Constant in Amides, Thioamides and Amidines. *J. Phys. Chem.* **1965**, *69*, 2570–2576. (b) Lunazzi, L.; Dondoni, A.; Barbaro, G.; Macciantelli, D. Conformational studies by dynamic NMR. IX. Activation Parameters for the Barrier to C-N Rotation in N,N-Dimethylbenzamidinium: A correction. *Tetrahedron Lett.* **1977**, *18*, 1079–1080.

(24) Stonehouse, J.; Adell, P.; Keeler, J.; Shaka, A. J. Ultrahigh-Quality NOE Spectra. *J. Am. Chem. Soc.* **1994**, *116*, 6037–6038.

(25) Kupce, E.; Boyd, J.; Campbell, I. D. Short Selective Pulses for Biochemical Applications. *J. Magn. Reson., Ser. B* **1995**, *106*, 300–303.

(26) Gunasekaran, P.; Perumal, S.; Menéndez, J. C.; Mancinelli, M.; Ranieri, S.; Mazzanti, A. Axial Chirality of 4-Arylpyrazolo[3,4-b]pyridines. Conformational Analysis and Absolute Configuration. *J. Org. Chem.* **2014**, *79*, 11039–11050.

(27) Brown, J. H.; Bushweller, C. H. *QCPE Bulletin, Bloomington, Indiana*, 1983; vol 3, p 103. A copy of the program is available on request from the authors (A.M. and M.M.).

(28) *Gaussian 09*, rev D. . 01. Frisch, M. J.; Trucks, G. W.; Schlegel, H. B.; Scuseria, G. E.; Robb, M. A.; Cheeseman, J. R.; Scalmani, G.; Barone, V.; Mennucci, B.; Petersson, G. A.; Nakatsuji, H.; Caricato, M.; Li, X.; Hratchian, H. P.; Izmaylov, A. F.; Bloino, J.; Zheng, G.; Sonnenberg, J. L.; Hada, M.; Ehara, M.; Toyota, K.; Fukuda, R.; Hasegawa, J.; Ishida, M.; Nakajima, T.; Honda, Y.; Kitao, O.; Nakai, H.; Vreven, T.; Montgomery, J. A., Jr.; Peralta, J. E.; Ogliaro, F.; Bearpark, M.; Heyd, J. J.; Brothers, E.; Kudin, K. N.; Staroverov, V. N.; Kobayashi, R.; Normand, J.; Raghavachari, K.; Rendell, A.; Burant, J. C.; Iyengar, S. S.; Tomasi, J.; Cossi, M.; Rega, N.; Millam, N. J.; Klene, M.; Knox, J. E.; Cross, J. B.; Bakken, V.; Adamo, C.; Jaramillo, J.; Gomperts, R.; Stratmann, R. E.; Yazyev, O.; Austin, A. J.; Cammi, R.; Pomelli, C.; Ochterski, J. W.; Martin, R. L.; Morokuma, K.; Zakrzewski, V. G.; Voth, G. A.; Salvador, P.; Dannenberg, J. J.; Dapprich, S.; Daniels, A. D.; Farkas, O.; Foresman, J. B.; Ortiz, J. V.; Cioslowski, J.; Fox, D. J.; Gaussian, Inc.: Wallingford CT, 2009.

(29) Zhao, Y.; Truhlar, D. G. The M06 Suite of Density Functionals for Main Group Thermochemistry, Thermochemical Kinetics, Noncovalent Interactions, Excited States, and Transition Elements: Two New Functionals and Systematic Testing of Four M06-class Functionals and 12 other Functionals. *Theor. Chem. Acc.* **2008**, *120*, 215–241.

(30) *GaussView 5.0.9*; Gaussian Inc.: Wallingford CT, 2009.

(31) Ikegai, K.; Mukaiyama, T. Synthesis of N-Aryl Pyridin-2-ones via Ligand Coupling Reactions Using Pentavalent Organobismuth Reagents. *Chem. Lett.* **2005**, *34*, 1496–1497.

(32) Kalyani, D.; Dick, A. R.; Anani, W. Q.; Sanford, M. S. Scope and Selectivity in Palladium-catalyzed Directed C–H bond Halogenation Reactions. *Tetrahedron* **2006**, *62*, 11483–11498.

(33) Kalyani, D.; Dick, A. R.; Anani, W. Q.; Sanford, M. S. A Simple Catalytic Method for the Regioselective Halogenation of Arenes. *Org. Lett.* **2006**, *8*, 2523–2526.

(34) Link, N. P.; Diaz, J. E.; Orelli, L. R. An Efficient Synthesis of N-Arylputrescines and Cadaverines. *Synlett* **2009**, *5*, 751–754.